Nano Research
2024, 17(6): 5661–5669

ISSN 1998-0124 CN 11-5974/O4
https://doi.org/10.1007/s12274-024-6490-z

Research Article

# Coupling metal-organic frameworks and wood-based carbon for water remediation

Akhter Zia[1,§], Manish Neupane[2,§], Aidan McGlone[1,§], Rui He[3], Ruikun Xin[4], Yifeng Liu[5], Qiangu Yan[6], Jinwu Wang[6], Ling Li[7], Zhiyong Cai[6], Pei Dong[3] (✉), and Yingchao Yang[1,2] (✉)

[1] *Department of Mechanical Engineering, University of Maine, Orono, ME 04469, USA*
[2] *Department of Mechanical and Aerospace Engineering, University of Missouri, Columbia, MO 65211, USA*
[3] *Department of Mechanical Engineering, George Mason University, Fairfax, VA 22030, USA*
[4] *Department of Civil and Environmental Engineering, Rice University, Houston, TX 77005, USA*
[5] *Department of Materials Science and NanoEngineering, Rice University, Houston, TX 77005, USA*
[6] *Forest Products Laboratory, USDA, Madison, WI 53726, USA*
[7] *School of Forestry Resources, University of Maine, Orono, ME 04469, USA*
[§] *Akhter Zia, Manish Neupane, and Aidan McGlone contributed equally to this work.*



**Received:** 29 September 2023 / **Revised:** 5 January 2024 / **Accepted:** 15 January 2024

## ABSTRACT

Fresh and clean water is highly demanded throughout the world. To effectively address the need, nanomaterials enabled nanotechnology has been explored as a means of more efficient, reliable, and environmentally friendly approach towards water treatment practices. One concern in adopting nanomaterials is how to retrieve them from water body to avoid secondary contamination. In this work, the earth abundant and sustainable wood, e.g., basswood, was selected and carbonized into porous carbon as host skeleton, and metal-organic frameworks (MOFs), e.g., MOF-199 with extremely high surface area, were grown throughout all channels in the porous basswood carbon. Targeting the traditional organic pollutant, methyl orange (MO), the combination of MOFs and basswood carbon (MOFs@carbon) demonstrates a remarkable adsorption capacity, which is 243% and 454% higher than basswood carbon and MOF-199, respectively. Such an outstanding adsorption performance originates from that the positively charged carbon pulls MO molecules close to carbon surface, leading to a high MO molecule concentration, and then the concentration gradient drives the MO molecules to be stored inside MOFs, functioning like pockets. These findings highlight the potential application of coupled MOFs and biomass carbon in addressing water remediation.

## KEYWORDS

metal-organic framework (MOF)-199, basswood carbon, MOFs@carbon, methyl orange

## 1 Introduction

The 2019 World Water Development Report highlighted that approximately two-thirds of the global population experiences severe water shortage for at least one month every year [1, 2]. One of the major detriments is water pollution, which arises from a combination of natural processes and human activities [3]. To address the limited availability of fresh and clean water sources, it is crucial to prioritize treatment of polluted water for reuse. Currently, various physical and chemical strategies have been developed. Conventional water treatment typically involves multi-step processes, including removal of coarse solids, sedimentation, flotation, and biological treatment. Advanced water treatment system combines various processes together, such as physicochemical [2], biological [4], chemical [4], and physical methods [5], along with filtration devices as tertiary treatment [5]. However, these advanced systems often require toxic chemicals, lead to potential secondary pollution, need larger installation space, and run at high cost [6]. In recent years, nanomaterials enabled nanotechnology has been explored as a means of more efficient, reliable, and environmentally friendly approach to overcome the limitations of existing technologies and contribute to sustainable water treatment practices [7–10].

Among various nanostructures, metal-organic frameworks (MOFs) have garnered considerable attention as a potential solution for water treatment. MOFs are a class of inorganic–organic hybrid materials where organic ligands are interconnected by metal ions or polynuclear metal clusters through coordination bonds [11]. Varying the metal and ligand components in MOF structures leads to modulation of pore size, morphology, as well as physical and chemical properties. MOFs exhibit a high specific surface area and a significant fraction of voids relative to their total volume, resulting in high porosity. As a result, MOFs can host a substantial number of active sites [8], enabling efficient storage [12, 13], separation, or adsorption [11] of gases, liquids, or nanoparticles. The applicability of MOFs in the field of water treatment is of paramount importance as it presents a new opportunity to address the global freshwater crisis. Notably, a zirconium-based MOF called UiO-66 demonstrated successful water desalination through a membrane with exceptional rejection

Address correspondence to Pei Dong, pdong3@gmu.edu; Yingchao Yang, yingchao.yang@missouri.edu

capabilities against multivalent ions. The membrane exhibited remarkable chemical stability, remaining non-degradable up to 170 h of usage [14]. Furthermore, a capacitive deionization electrode composed of zeolitic imidazolate framework-67 (ZIF-67) and polypyrrole displayed excellent electrical conductivity and a high desalination capacity of 11.34 $mg \cdot g^{-1}$. The superior desalination performance was achieved due to the high porosity and electrical conductivity [15].

MOFs have been employed to remove organic pollutants from water [16–18]. In the context of adsorption, chromium-based MOFs, namely MIL-101, MIL-53, and protonated ethylenediamine-grafted MIL-101 (PED-MIL-101), have been investigated to eliminate methyl orange (MO) in water. It was observed that MIL-101 with larger pores exhibited superior adsorption compared with MIL-53 with smaller pores. Additionally, the electrostatic interaction between absorbent and MO exerted more influence than pore size, which was evidenced by the outstanding performance of PED-MIL-101. The cationic $-NH_3$ in PED-MIL-101 attracted the anionic $-SO_3$ group in MO, which enhanced the MO adsorption [17]. Additionally, MOF-199, also referred to as HKUST-1, was combined with activated carbon [19], silica matrices [20], and polyaniline [21] to enhance adsorption capability. Incorporating a small amount of activated carbon into MOF-199 can significantly increase the adsorption capacity of sulfur [19]. Among all water treatments using powder-like MOFs, one major challenge is to retrieve MOFs from the treated water body in case of secondary pollution.

In this study, an approach by coupling MOF-199 with basswood-converted porous carbon has been meticulously investigated. The MOF-199, known for its exceptional surface area and porous structure, provides numerous active sites and ample space for capturing organic compounds, while the basswood-converted porous carbon acts as a host for MOFs, facilitating the retrieval of nanomaterials from the water body. With a specific target on MO, the combination of MOFs and basswood carbon (MOFs@carbon) demonstrates a remarkable adsorption capacity, 243% and 454% higher than pristine basswood carbon and MOF-199, respectively. As the MO solution is within the pH values of 3.1–4.4, the basswood carbon behaves positively charged, which facilitates the attraction of MO molecules to the surface of carbon. Subsequently, the MOFs grow on the carbon function as pockets, effectively adsorbing MO molecules around the carbon. These findings highlight the application of coupled MOFs and biomass carbon in addressing water pollution.

## 2 Experimental

### 2.1 Materials

Copper nitrate trihydrate ($Cu(NO_3)_2 \cdot 3H_2O$, 99% for analysis, Fisher Chemical), 1,3,5-benzenetricarboxylic acid ($H_3BTC$, > 98.0%(T), Tokyo Chemical Industry), N,N-dimethylformamide (DMF, certified ACS, Fisher Chemical), ethanol (Fisher Chemical), sulfuric acid (Fisher Chemical), hydrogen peroxide (34%–37%, Fisher Chemical), nickel nitrate hexahydrate (98%, Thermo Scientific Chemicals), methyl orange (MO, Sigma-Aldrich), basswood, and argon gas (ultrahigh purity, Spec Air Specialty Gases) were purchased from different vendors and used without any further purification.

### 2.2 Basswood to carbon

The basswood was sliced into approximately 25 mm × 25 mm × 3 mm which was placed into a tube furnace (VTF-SH1200-D50L800) for carbonization. Under argon gas protection, the pieces were heated to 250 °C for 6 h and then carbonized at 1000 °C for another 6 h. After cooling to room temperature, the porous carbon was taken out, sanded with 800 grit sandpaper, and then finely polished with 3000 grit sandpaper down to 1 mm in thickness. The porous carbon sheets were initially cleaned in deionized (DI) water, and then in ethanol via a sonication bath until ethanol was free of carbon particles.

### 2.3 Piranha treatment

The piranha solution was prepared by mixing sulfuric acid and hydrogen peroxide in a ratio of 3:1. The hydrogen peroxide was added to the sulfuric acid slowly and mixed via sonication. The carbon sheets were etched in the solution for 24 h, and then thoroughly washed with DI water until the pH value of the water was approximately 7.

### 2.4 Nickel impregnation

The porous carbon sheets were soaked in a 0.25 M nickel nitrate solution for 48 h. The carbon sheets were first heated to 800 °C under argon gas to get nickel oxide particles, and then reduced at 800 °C under a mixed gas of hydrogen and argon in a ratio of 1:4 with a flow rate of 200 sccm for 1 h to obtain nickel nanoparticles on the porous carbon. After thermal treatment, the furnace was shut down and the specimen was cooled down to room temperature with continuous flow of the mixed gas.

### 2.5 MOF-199 synthesis

MOF-199 was synthesized using a similar method as reported [22]. Firstly, 22.5 mL dimethylformamide, 22.5 mL ethanol, and 1.5 g benzene tricarboxylic acid were mixed to form one solution. Secondly, another solution was made with 22.5 mL of DI water and 3.114 g copper nitrate trihydrate. And then, the solutions were mixed and stirred for 10 min. Finally, 50 mL solution was sealed into a 100 mL Teflon-lined autoclave, which was placed in an oven at 100 °C for 10 h. After the hydrothermal reaction, the powder was washed with DI water and ethanol twice.

### 2.6 MOF-199 growing in porous carbon (MOFs@carbon)

To grow MOF-199 inside the porous carbon sheets, the carbon sheets with Ni impregnation were immerged into the solution mentioned above, followed by degassing with an air pump. After soaking and degassing, the carbon sheets together with the solution were sealed into the Teflon-lined autoclave for MOF-199 growth in an oven at 100 °C for 10 h. The basswood carbon with MOFs was labeled as MOFs@carbon.

### 2.7 Characterization

For all MOF-199, porous carbon sheets, and MOFs@carbon specimens, morphology and composition were characterized by scanning electron microscopy (SEM, Zeiss NVision 40 FIB/SEM). The content and configuration of carbon and oxygen were analyzed by X-ray photoelectron spectroscopy (XPS) (PHI Quanter XPS with Al K$\alpha$ X-ray). All specimens were analyzed under ABB-Bomem FTLA 2000 Fourier transform infrared (FTIR) spectrometer before and after adsorption of MO to investigate the bonding between the specimens and MO. A DVS Advanced Analysis Suite was used to measure the Brunauer–Emmett–Teller (BET) surface area.

### 2.8 Evaluation of MO adsorption

Adsorption testing was performed with 6 $mg \cdot L^{-1}$ MO solution. The MOF-199, carbon, or MOFs@carbon were placed in a small glass vial with 2 mL of solution and allowed to sit until the solution color remained constant. The adsorption of MO by MOF-199, porous carbon sheets, and MOFs@carbon was

measured using a GENESYS 150 ultraviolet–visible (UV–vis) spectrophotometer over the range of 300–600 nm. The data were collected from the 464 nm wavelength as it was close to the maximum absorption wavelength of 465 nm for MO.

## 3 Results and discussion

Figure 1 schematically demonstrates approaches to remove organic pollutants from water. Generally, chemical powders composed of activated carbon or other absorbent materials, e.g., MOFs, are directly dispensed into water body and interact with pollutants, e.g., MO, as shown in Fig. 1(a). As they cannot be retrieved or separated from the treated water, a risk of secondary contamination remains due to the presence of these residual chemical powders. If the chemical powders are held in a porous framework (Fig. 1(b)), the materials would be easily reclaimed from water after adsorption, avoiding secondary contamination.

For the porous framework, the abundant forest resources provide cost-competitive sustainable materials. After carbonization, wood can be converted into porous carbon. The morphology of wood carbon depends on the cell type, size, shape, and wall-to-lumen ratio among tree species. Among all woods, basswood has a medium weight (~ 416 kg·m$^{-3}$), allowing the converted carbon to have a great specific mechanical strength. Meanwhile, basswood may have a trunk diameter up to 1.2 m [23, 24], suggesting that the porous carbon can be scaled up for advanced applications. When basswood is sliced along the longitudinal direction of growth, a uniform porous structure without crossing annual growth rings will be obtained.

Figure 2 demonstrates the morphologies of basswood sheet before and after carbonization, as well as the growth of MOFs in all channels. Generally, wood is carbonized under a temperature range of 500–1000 °C. Lower temperature may facilitate to reserve certain functional groups. To avoid the contribution from functional groups to MO adsorption, basswood was carbonized at 1000 °C. Figures 2(a)–2(c) show optical images of radially cut basswood sheet, carbonized basswood, and carbonized basswood with MOFs grown on the surface. After cutting, pores in basswood may collapse, which would block the MOF precursor to flow into channels. To avoid this, both top and bottom surfaces of porous carbon sheets were carefully polished (Fig. 2(b)) to expose all pores shown in Fig. 2(d). Such neat morphology will allow full interaction between all carbon surface and MOF precursor solution to facilitate the growth of MOFs. The blue color in Fig. 2(c) indicates that MOFs fully cover the basswood carbon surfaces. To check the internal morphology of basswood carbon and distribution of MOFs in channels. Figures 2(d)–2(f) show SEM images of basswood carbon in radial and longitudinal directions. Basswood has both small and large pores distributed across the radial direction (Fig. 2(d)). Small pores have a size ranging from 5 to 20 μm, whereas large pores are between 40 and 65 μm in width. The longitudinal channel is smooth with patterned ridges along the radial direction evidenced in Fig. 2(e). The higher magnification SEM image in Fig. 2(f) highlights the presence of pores along the longitudinal direction. These pores will allow the flow of MOF precursor among channels. Figures 2(g) and 2(h) confirm that the grown MOFs are uniformly distributed throughout the channels and have a high density. During the growth of MOFs, the period of degassing porous carbon immersed into MOF precursor is critical to the loading rate of MOFs. Figure S1 in the Electronic Supplementary Material (ESM) shows the MOFs grown on surface and in channels of bass carbon with different immersion periods. Once the bass carbon is immersed into MOF precursor, MOFs can easily nucleate and grow on carbon surface. There is no difference whether the period of immersion is short or long. The precursor can feed well to the MOF growth. However, the growth condition is different in bass carbon channels. If air is trapped inside, the MOF precursor will

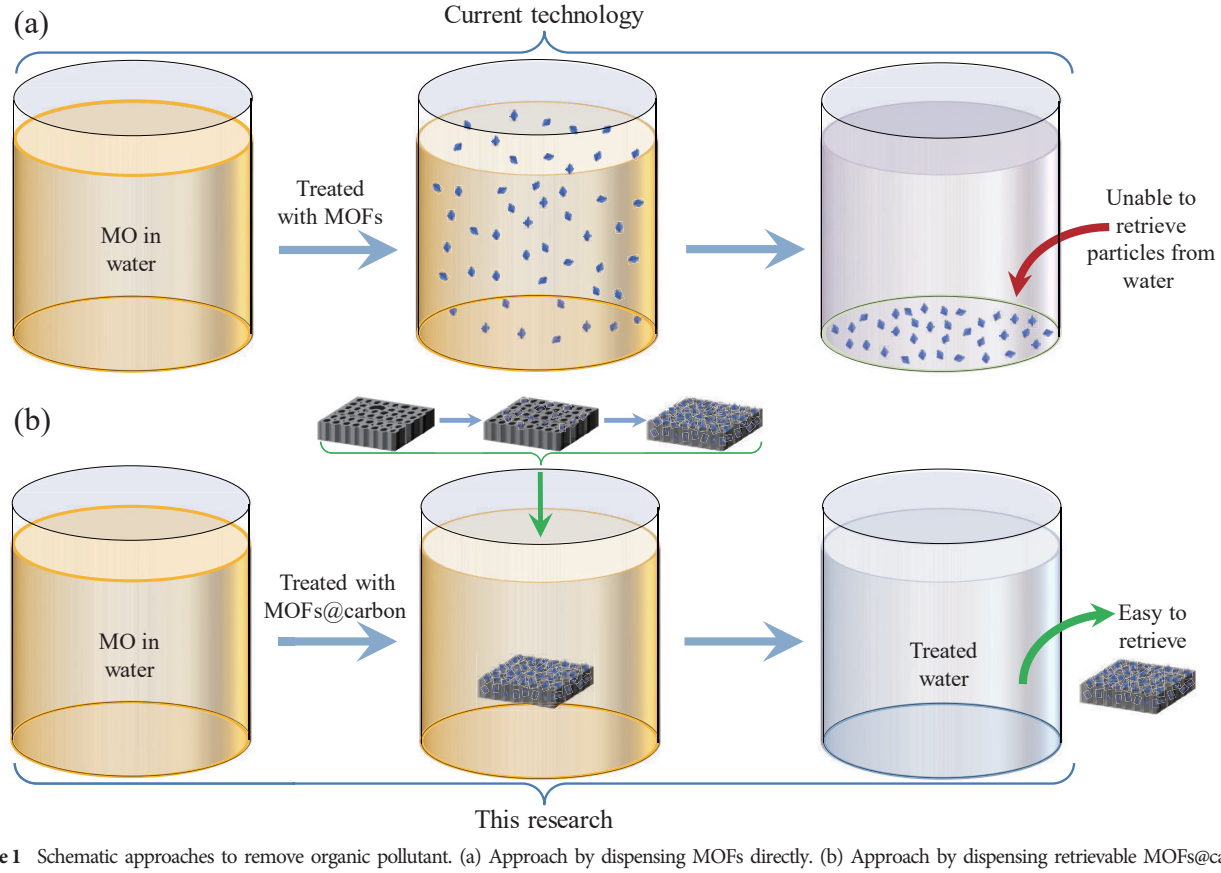


**Figure 1** Schematic approaches to remove organic pollutant. (a) Approach by dispensing MOFs directly. (b) Approach by dispensing retrievable MOFs@carbon, avoiding secondary contamination.

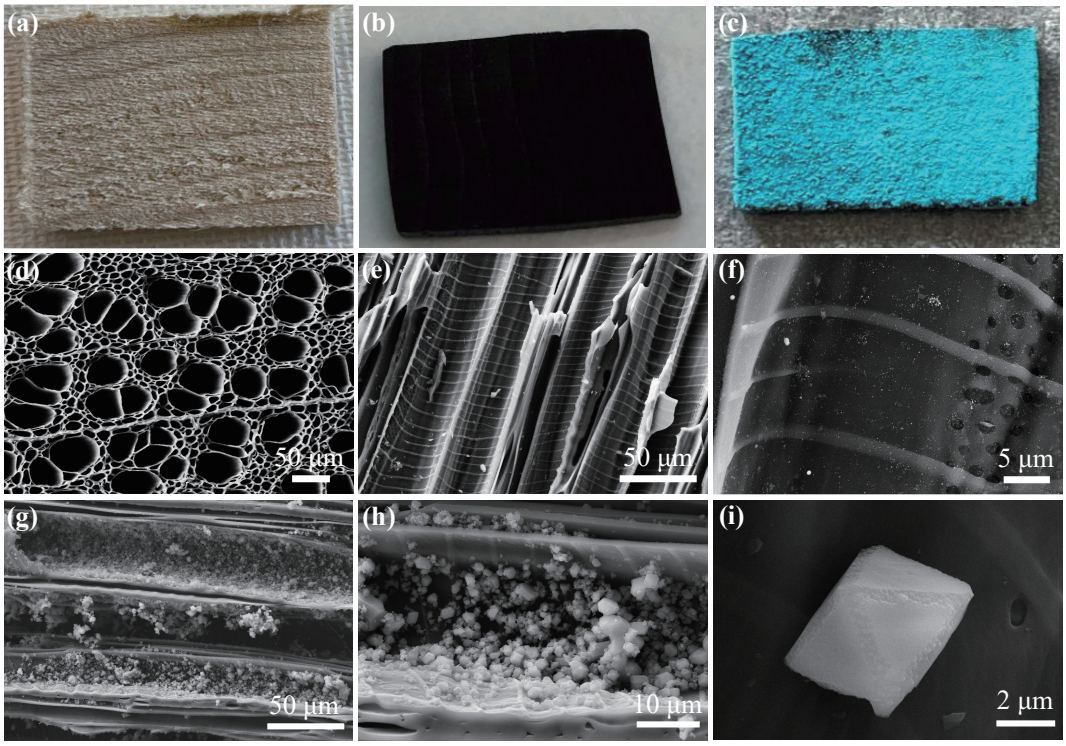


**Figure 2** Morphology of basswood, basswood carbon, and basswood carbon with MOF-199. Optical images of (a) basswood sheet, (b) polished basswood carbon sheet, and (c) MOFs@carbon sheet. ((d)–(f)) SEM images of basswood converted carbon: (d) top view, (e) cross-sectional view, and (f) fine pores in the wall. ((g) and (h)) Low-magnification SEM images of grown MOFs@carbon. (i) Individual MOF-199 particle.

be unable to reach inner surface of pores and channels, leading to no or sparse growth of MOFs. Once the degassing is over 24 h, the growth in all channels is quite uniform. The high-density MOFs with uniform distribution across carbon sheets will greatly increase the surface area and further aid water remediation. Individual MOF-199 particles have an octahedral shape with a diagonal length of approximately 6 μm, as shown in Fig. 2(i).

MOFs are highly porous and possess exceptional surface area. Combining MOFs with basswood carbon will greatly increase surface area compared with the solely basswood carbon. Meanwhile, basswood carbon will be an excellent host for MOFs as it has a great number of channels with open pores passing through neighbor channels. To measure the surface area, BET analysis was performed. The plots and discussion for $N_2$ adsorption/desorption isotherms and Barrett–Joyner–Halenda (BJH) pore size distributions of MOFs, basswood carbon, and MOFs@carbon can be found in Section S2 and Fig. S2 in the ESM. Table 1 lists the specific surface area of three materials. MOF-199 has an exceptional surface area of 1188.4 $m^2 \cdot g^{-1}$, whereas basswood carbon exhibits only 4.5 $m^2 \cdot g^{-1}$. For MOFs@carbon, the surface area is compromised to 651.7 $m^2 \cdot g^{-1}$, which results from the weight ratio 1:1 of MOFs to carbon in MOFs@carbon. Both MOFs and MOFs@carbon have similar and small pore width, approximately 1 nm, while basswood carbon has slightly large average pore size, 1.6 nm.

To learn the water remediation potential of MOFs@carbon, MO was used as a representative pollutant, which was treated by MOF-199, basswood carbon, and MOFs@carbon. Based on the solution color change, the level of residual MO in water can be easily visualized. Figure 3(a) shows an optical image of 6 $mg \cdot L^{-1}$ MO solution in a glass vial, the color of which can be used as a benchmark. Firstly, MOF-199 was added into another 2 mL MO solution and left in the dark until the color of the solution was stable three days later. Figure 3(b) shows the light-orange solution, indicating that MO was adsorbed by MOFs. Secondly, with the same procedure, the MO solution treated by basswood carbon has a pale orange color, which suggests less MO residual compared with that treated by MOFs. Finally, the last batch of MO solution was treated by MOFs@carbon. The MO was almost completely adsorbed, as indicated by the colorless solution in Fig. 3(d). Although the mass of three absorbents is the same, interestingly, the coupled MOFs and porous carbon work better than individual materials. To quantify the residual MO, all three solutions were measured by a UV–vis spectrometer at the maximum absorption wavelength of MO (465 nm). Figure 3(e) shows that 80.3% MO remained in the solution treated by MOF-199 only, and in contrast, 63.2% MO was not adsorbed in the solution treated by basswood carbon. Astonishingly, there is only 10.5% MO remained in the solution after MOFs@carbon treatment, demonstrating a significant improvement over either adsorbent used alone. With a simple assumption, 25 mg MOF-199 and 25 mg basswood carbon were used to treat 2 mL MO solution, and the adsorption capacity towards MO would be approximately 28.3%, which is less than one third of 89.5%, the adsorption capacity of 50 mg MOFs@carbon. The hidden synergistic mechanism will be detailed in the later section. To trace MO adsorption rate by MOFs@carbon, the MO concentration at several periods was measured and summarized in Fig. 3(f). The

**Table 1** BET specific surface area of MOF-199, basswood carbon, and MOFs@carbon

| Materials | Surface area ($m^2 \cdot g^{-1}$) | Pore volume ($cm^3 \cdot g^{-1}$) | Pore width (nm) |
|---|---|---|---|
| MOF-199 | 1188.4 | 0.63 | 1.06 |
| Basswood carbon | 4.5 | 0.004 | 1.58 |
| MOFs@carbon | 651.7 | 0.35 | 1.08 |

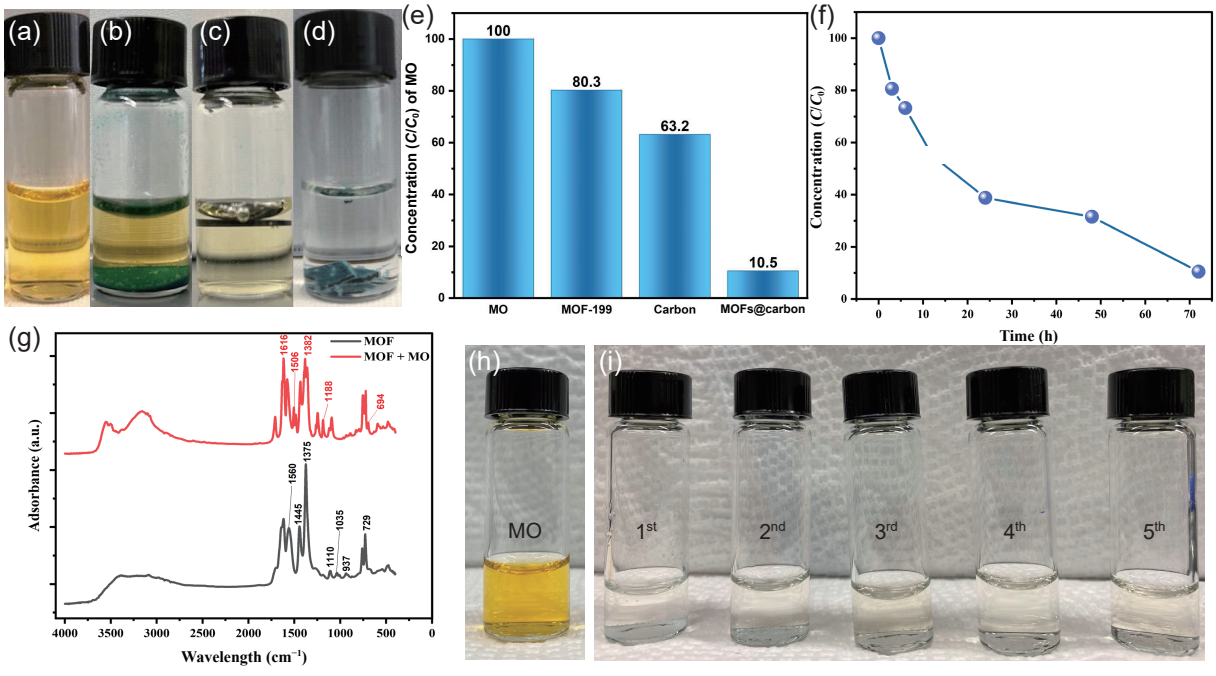


**Figure 3** Testing and characterization of MO solutions (2 mL) treated by 50 mg basswood carbon, MOF-199, and MOFs@carbon individually for three days. (a) Reference MO solution with concentration of 6 mg·L$^{-1}$. (b) Solution treated by MOF-199. (c) Solution treated by basswood carbon. (d) Solution treated by MOFs@carbon. (e) Quantification of residual MO in three solutions. (f) Concentration vs. time plot for MO solution treated by MOFs@carbon. (g) FTIR spectra for MOF-199 before and after MO adsorption. (h) Digital image of MO solution before adsorption. (i) Reusability and stability of MOFs@carbon towards MO removal.

slope for the curve within 12 h is much higher than that after 12 h, suggesting that the MO adsorption rate is high at the beginning. With MO molecules adsorbed, the concentration gradient of MO molecules inside and outside MOF 199 and porous carbon gets lower, reducing the driving force for MO molecules to occupy the remaining space in MOFs@carbon. Approximately 50% MO can be adsorbed within the first 12 h. Given 38 and 72 h, the remaining MO reached around 30% and 10%, respectively. The MO adsorption achieved by MOFs@carbon is superior to previously reported similar materials, such as ZIF-67 and UiO-66 (Table 2) [25–32]. Other materials like chitosan-based nanocomposites may have a decent adsorption result, but lack the retrievability of the adsorbent, posing a risk of secondary contamination [27, 33]. The removal of MOFs@carbon from water is easy. No filtration or any form of purification method is needed, avoiding secondary pollution from the used MOF particles. In terms of the versatility of MOFs@carbon, MOF-199 has been utilized for the removal of polar molecular species such as phenol and indole. This efficacy is attributed to the strong interaction between the respective polar –OH and N–H groups with $Cu^{2+}$ [34]. Additionally, MOF-199 hybrids have demonstrated the capability to eliminate rhodamine-6G (Rh6G), a cationic dye, as well as basic blue 41, a photocatalytic dye, and benzene vapor [35–37]. These findings collectively suggest that MOFs@carbon exhibit promising potential for the removal of various organic compounds among the specific examples investigated.

To further understand the adsorption of MO molecules in MOF-199, FTIR analysis on MOF-199 before and after adsorption of MO was studied. A characteristic peak at 726 cm$^{-1}$ can be ascribed to the stretching vibration of Cu–O presented in MOF-199 [22, 38, 39]. The peaks around 1375 and 1445 cm$^{-1}$ are the stretching vibration of C–O and bending vibration of OH, respectively [22, 39, 40]. A broad hump between 3000 and 3600 cm$^{-1}$ originates from vibrational OH in water [22]. After MO adsorption, a prominent peak is detected at 694 cm$^{-1}$ [41, 42], and the peak at 1382 cm$^{-1}$ shifted from 1375 cm$^{-1}$, which are from the MO (sulphonic group) and due to adsorbed MO in MOF-199,

**Table 2** Adsorption efficiency of MO by different adsorbents

| Adsorbent | Removal efficiency (%) | Ref. |
|---|---|---|
| Activated carbon from pop corn | 48.5 | [28] |
| Activated carbon from waste tire rubber | 80 | [29] |
| Zirconium MOF (UiO-66) | 31 | [30] |
| Cadmium MOFs | 39 | [31] |
| ZIF-67 | 68.5 | [25] |
| Ni dopped ZIF-67 | 82.9 | [25] |
| Amino groups functionalized UiO-66 MOF | 87.4 | [26] |
| Chitosan-montmorillonite composite | 94.6 | [32] |
| Chitosan-lysozyme biocomposite | 52.8 | [27] |
| Activated carbon from basswood | 36.8 | This work |
| MOF-199 | 19.7 | This work |
| MOFs@carbon | 89.5 | This work |

respectively. The peak located at 3000 $cm^{-1}$ can be assigned to $CH_3$ stretching vibration from MO [43].

To assess the reusability and stability of MOFs@carbon for MO removal, cyclic adsorption and desorption of MO were performed. Figure 3(h) shows a digital image of MO solution before treatment. The concentration of MO is 6 $mg·L^{-1}$, the color of which was used as the benchmark. For each cyclic adsorption, a piece of MOFs@carbon was dropped into the MO solution. After 24 h, the specimen was retrieved. To desorb MO in the MOFs@carbon, ethanol and 0.05 N $HNO_3$ were used to wash the specimen followed by DI water wash. The desorbed MOFs@carbon was then used to conduct the second cycle of adsorption and thereafter. Digital images were taken for each solution after retrieving the MOFs@carbon and shown in Fig. 3(i). All solutions are visibly colorless or in a pale-yellow color, indicating that most of MO was removed successfully after each cycle. The cyclic reusability and stability are consistent for MOFs@carbon towards MO adsorption.

In addition to reusability and stability, the effect of loading rate of MOFs on carbon towards the MO removal efficiency was evaluated as well. The MO solution was adsorbed by MOFs@carbon with carbon soaked into MOF precursor for 24, 12, and 6 h. More details can be found in Section S3 and Fig. S3 in the ESM. Notably, the colorless solution, resulted from MOFs@carbon featuring carbon soaked in the MOF precursor for 24 h, demonstrated effective MO adsorption. Hence, achieving comprehensive coverage of MOFs within channels and on the surface is deemed preferable for the efficient removal of organic compounds.

As elaborated by the UV–vis spectrophotometer, MOFs@carbon exhibits synergetic effect in MO adsorption. The obtained performance is much better than those of individual MOF-199 and basswood carbon. Surface charge on basswood carbon may promote MO adsorption. Depending on the pH value of working solutions into which carbon is immersed, the surface charge of the carbon can be either positive or negative [44–46]. If the pH value of the solution is lower than the pH zero point of charge (pHzpc), the surface of the carbon is positive. On the other hand, the negatively charged carbon can be obtained in the working solution with pH value higher than the pHzpc [44, 46]. MO is a weak acid and has a pH ranging from 3.1 to 4.4 in an aqueous solution [47], while the pHzpc of the carbon is reported to be higher than 5 [44, 48, 49] and the pH of the basswood carbon was also measured to be higher than 5 after acid treatment followed by a few washes. Therefore, the basswood carbon in MO aqueous solution is positively charged. For MO, it contains a negatively charged sulfate group which electrostatically interacts with a positively charged adsorbent [17]. With this understanding, the attraction force lacks between MO and MOF (Fig. 4(a)) and is present between MO and basswood carbon (Fig. 4(b)), accounting for the difference in MO adsorption capacity: 19.7% and 36.8% of MO in solutions can be adsorbed by MOFs and basswood carbon, respectively (Fig. 3(e)). For MOFs@carbon schematically demonstrated in Fig. 4(c), positively charged carbon pulls MO molecules close to carbon surface, resulting in a high MO molecule concentration. MOFs growing on carbon surface function like pockets. As the MO concentration outside MOFs is higher than that inside, the concentration gradient drives the MO

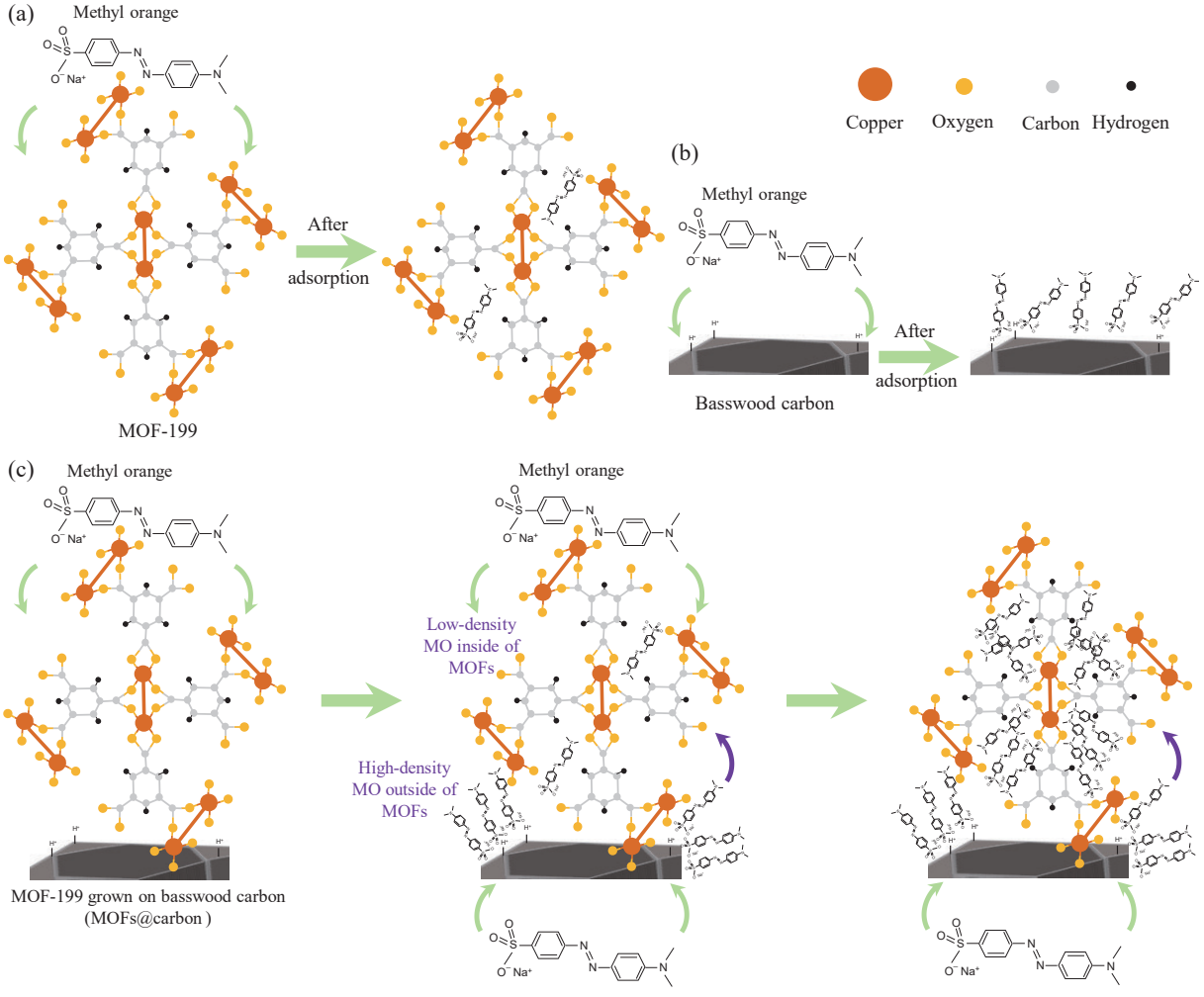


**Figure 4** Schematics for adsorption mechanisms. Adsorption of MO by (a) MOF-199, (b) basswood carbon, and (c) MOFs@carbon.

molecules to be stored inside MOFs. Only the combined basswood carbon and MOFs can achieve such a synergistic working mechanism, largely promoting the MO adsorption capacity.

XPS analysis was conducted on basswood carbon, MOF-199, and MOFs@carbon before and after MO adsorption to investigate if the adsorption is physical or chemical. Figure 5 shows the deconvoluted C 1s core level spectra for all six specimens. Figure 5(a) shows C 1s spectrum of basswood carbon can be deconvoluted into three typical Gaussian curves with peaks at 284.8, 285.6, and 286.5 eV, corresponding to C–C ($sp^2$), C–C ($sp^3$), and C–O, respectively. The $sp^3$ bond may result from defects due to high temperature treatment. The C–C $sp^3$ peak is not visible in MOFs@carbon (Fig. 5(c)) and basswood carbon after MO adsorption (Fig. 5(d)), suggesting that defect signals were blocked by the uniform coverage of MOFs on basswood carbon and adsorbed MO, respectively. As shown in Figs. 5(d)–5(f), no new peak and no big shift are found among all spectra after MO adsorption, suggesting that the bonding between MO and adsorbents is physical. To theoretically confirm the adsorption mechanism, both first-order pseudo-kinetic model [50] and second-order pseudo-kinetic model [51] were applied to MO adsorption by MOFs@carbon. The detailed calculations and results can be found in Section S4 in the ESM. The experimental measurement of MO residual upon time was plotted against the calculated relationship between MO residual $q_t$ and time $t$, with the calculated pseudo-first-order adsorption rate constant $k_1$ and pseudo-second-order adsorption rate constant $k_2$. Figure S4 in the ESM shows that the experimental measurement closely aligns with the plots generated by the second-order pseudo-kinetic model using the calculated $k_2$, rather than the first-order pseudo-kinetic model using the calculated $k_1$, suggesting that the kinetics of MO removal by MOFs@carbon is a diffusion-controlled process [52]. Such adsorption mechanism is driven by the gradient of MO concentration in and out of MOFs.

## 4 Conclusions

As a large population experiences severe water shortage majorly due to water pollution, it is crucial to prioritize treatment of polluted water for fresh and clean water. Nanomaterials have greatly been adopted for water treatment. Among various nanostructures, MOFs have garnered considerable attention due to their high specific surface area and a significant fraction of voids relative to their total volume, resulting in high porosity. To well reclaim the nanostructures, the basswood-converted porous carbon acts as a host for MOFs, facilitating the retrieval of materials from the water body. With a specific target on MO, the combination of MOFs and basswood carbon demonstrates a remarkable adsorption capacity. Briefly, only 19.7% and 36.8% MO can be adsorbed by MOF-199 and basswood carbon, respectively. Astonishingly, 89.5% MO can be removed after MOFs@carbon treatment, demonstrating a significant improvement over either adsorbent used alone. As the basswood carbon is positively charged, it pulls negatively charged MO molecules closer to the carbon surface, resulting in a high MO molecule concentration. The MO concentration gradient drives the MO molecules to be stored inside MOFs, largely promoting the MO adsorption capacity. Only the combined carbon and MOFs can achieve such synergistic working mechanism. The research sheds light on coupling sustainable wood and advanced porous nanostructures MOFs for water treatment including water remediation and desalination.

## Acknowledgements

J. W. W., Z. Y. C., and Y. C. Y. acknowledge the financial support from the USDA Forest Service (No. 20-JV-11111124-035). Y. C. Y. and P. D. acknowledge the financial support from the Department of the Interior, Bureau of Reclamation (No. R19AC00116). Y. C. Y. thanks Dr. Y. Q. Meng in Idaho National Laboratory for helping on BET measurement.

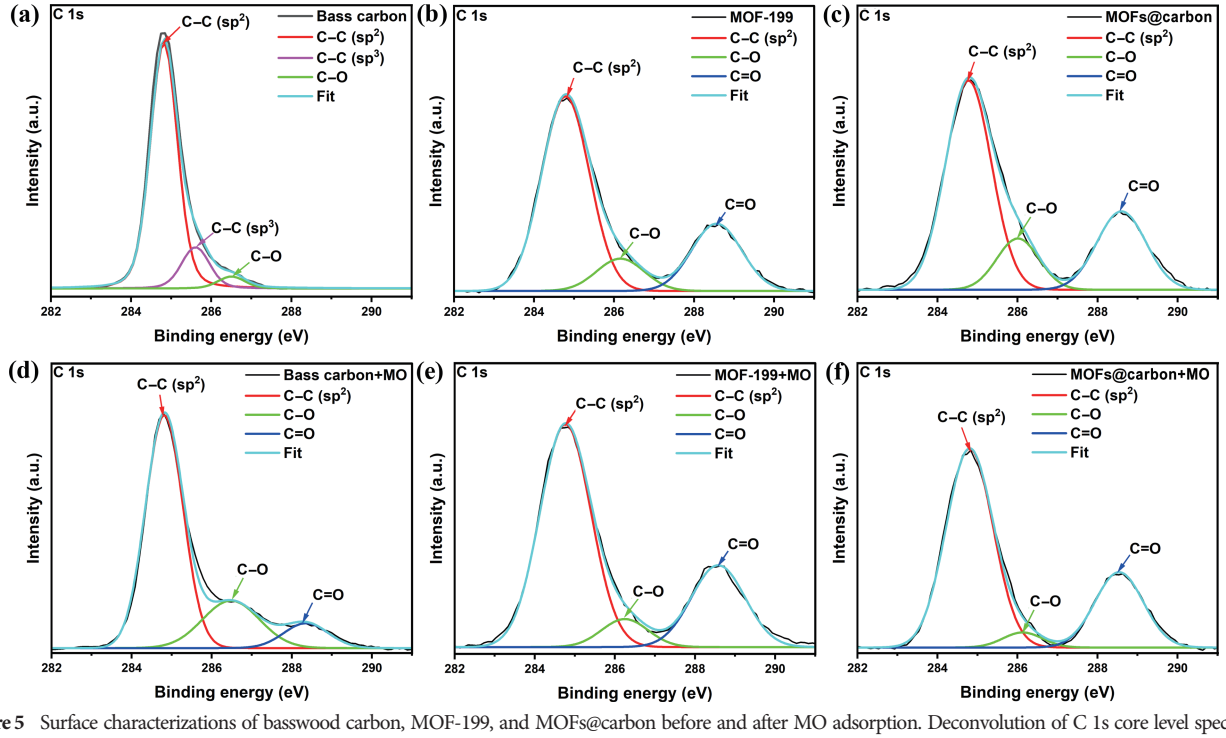


**Figure 5** Surface characterizations of basswood carbon, MOF-199, and MOFs@carbon before and after MO adsorption. Deconvolution of C 1s core level spectra of (a) basswood carbon impregnated with NiO, (b) MOF-199, (c) MOFs@carbon, (d) basswood carbon with adsorbed MO, (e) MOF-199 with adsorbed MO, and (f) MOFs@carbon with adsorbed MO.

**Electronic Supplementary Material:** Supplementary material (investigation of MOF loading rate on bass carbon, BET measurement on three absorbents, MO removal efficiency upon MOF loading rates, and calculations towards MO adsorption mechanism) is available in the online version of this article at https://doi.org/10.1007/s12274-024-6490-z.

## References


[1] Pooja, D.; Kumar, P.; Singh, P.; Patil, S. *Sensors in Water Pollutants Monitoring: Role of Material*; Springer: Singapore, 2020.

[2] Nie, C. Y.; Wang, J. L.; Cai, B. H.; Lai, B.; Wang, S. B.; Ao, Z. M. Multifunctional roles of $MoS_2$ in persulfate-based advanced oxidation processes for eliminating aqueous organic pollutants: A review. *Appl. Catal. B: Environ.* **2023**, *340*, 123173.

[3] Stefanakis, A. I.; Zouzias, D.; Marsellos, A. Groundwater pollution: Human and natural sources and risks. *Environ. Sci. Eng.* **2017**, *4*, 82–102.

[4] Hoang, A. T.; Pham, V. V.; Nguyen, D. N. A report of oil spill recovery technologies. *Int. J. Appl. Eng. Res.* **2018**, *13*, 4915–4928.

[5] Sonune, A.; Ghate, R. Developments in wastewater treatment methods. *Desalination* **2004**, *167*, 55–63.

[6] Crini, G.; Lichtfouse, E. Advantages and disadvantages of techniques used for wastewater treatment. *Environ. Chem. Lett.* **2019**, *17*, 145–155.

[7] Li, X.; Wang, B. Atomic regulations of single atom from metal-organic framework derived carbon for advanced water treatment. *Nano Res.* **2023**, *16*, 10326–10341.

[8] Vikrant, K.; Kumar, V.; Vellingiri, K.; Kim, K. H. Nanomaterials for the abatement of cadmium(II) ions from water/wastewater. *Nano Res.* **2019**, *12*, 1489–1507.

[9] Zhao, Y.; Song, X.; Huang, M.; Jiang, H.; Toghan, A. Crown ether interlayer-modulated polyamide membrane with nanoscale structures for efficient desalination. *Nano Res.* **2023**, *16*, 6153–6159.

[10] Hou, Y. Q.; Wang, M.; Chen, X. Y.; Hou, X. Continuous water–water hydrogen bonding network across the rim of carbon nanotubes facilitating water transport for desalination. *Nano Res.* **2021**, *14*, 2171–2178.

[11] Li, J. R.; Kuppler, R. J.; Zhou, H. C. Selective gas adsorption and separation in metal-organic frameworks. *Chem. Soc. Rev.* **2009**, *38*, 1477–1504.

[12] Liu, S., Sun, L. X., Xu, F., Zhang, J., Jiao, C. L., Li, F., Li, Z. B., Wang, S., Wang, Z. Q., Jiang, X. et al. Nanosized Cu-MOFs induced by graphene oxide and enhanced gas storage capacity. *Energy Environ. Sci.* **2013**, *6*, 818–823.

[13] Millward, A. R.; Yaghi, O. M. Metal-organic frameworks with exceptionally high capacity for storage of carbon dioxide at room temperature. *J. Am. Chem. Soc.* **2005**, *127*, 17998–17999.

[14] Liu, X. L.; Demir, N. K.; Wu, Z. T.; Li, K. Highly water-stable zirconium metal-organic framework UiO-66 membranes supported on alumina hollow fibers for desalination. *J. Am. Chem. Soc.* **2015**, *137*, 6999–7002.

[15] Wang, Z. M.; Xu, X. T.; Kim, J.; Malgras, V.; Mo, R.; Li, C. L.; Lin, Y. Z.; Tan, H. B.; Tang, J.; Pan, L. K. et al. Nanoarchitectured metal-organic framework/polypyrrole hybrids for brackish water desalination using capacitive deionization. *Mater. Horiz.* **2019**, *6*, 1433–1437.

[16] Tchinsa, A.; Hossain, M. F.; Wang, T.; Zhou, Y. B. Removal of organic pollutants from aqueous solution using metal organic frameworks (MOFs)-based adsorbents: A review. *Chemosphere* **2021**, *284*, 131393.

[17] Haque, E.; Lee, J. E.; Jang, I. T.; Hwang, Y. K.; Chang, J. S.; Jegal, J.; Jhung, S. H. Adsorptive removal of methyl orange from aqueous solution with metal-organic frameworks, porous chromium-benzenedicarboxylates. *J. Hazard. Mater.* **2010**, *181*, 535–542.

[18] Hasan, Z.; Choi, E. J.; Jhung, S. H. Adsorption of naproxen and clofibric acid over a metal-organic framework MIL-101 functionalized with acidic and basic groups. *Chem. Eng. J.* **2013**, *219*, 537–544.

[19] Shi, R. H.; Zhang, Z. R.; Fan, H. L.; Zhen, T.; Shangguan, J.; Mi, J. Cu-based metal-organic framework/activated carbon composites for sulfur compounds removal. *Appl. Surf. Sci.* **2017**, *394*, 394–402.

[20] Isaeva, V. I.; Chernyshev, V. V.; Fomkin, A. A.; Shkolin, A. V.; Veselovsky, V. V.; Kapustin, G. I.; Sokolova, N. A.; Kustov, L. M. Preparation of novel hybrid catalyst with an hierarchical micro-/mesoporous structure by direct growth of the HKUST-1 nanoparticles inside mesoporous silica matrix (MMS). *Microporous Mesoporous Mater.* **2020**, *300*, 110136.

[21] Jafari, E. A.; Moradi, M.; Borhani, S.; Bigdeli, H.; Hajati, S. Fabrication of hybrid supercapacitor based on rod-like HKUST-1@polyaniline as cathode and reduced graphene oxide as anode. *Phys. E Low Dimens. Syst. Nanostruct.* **2018**, *99*, 16–23.

[22] Lin, S.; Song, Z. L.; Che, G. B.; Ren, A.; Li, P.; Liu, C. B.; Zhang, J. S. Adsorption behavior of metal-organic frameworks for methylene blue from aqueous solution. *Microporous Mesoporous Mater.* **2014**, *193*, 27–34.

[23] Brush, W. D. *Utilization of Basswood*; Govt. Print. Off: Washington, 1922.

[24] Meier, E. *WOOD! Identifying and Using Hundreds of Woods Worldwide*; The Wood Database, 2015.

[25] Nazir, M. A.; Najam, T.; Zarin, K.; Shahzad, K.; Javed, M. S.; Jamshaid, M.; Bashir, M. A.; Shah, S. S. A.; Rehman, A. U. Enhanced adsorption removal of methyl orange from water by porous bimetallic Ni/Co MOF composite: A systematic study of adsorption kinetics. *Int. J. Environ. Anal. Chem.* **2023**, *103*, 4841–4856.

[26] Lv, S. W.; Liu, J. M.; Ma, H.; Wang, Z. H.; Li, C. Y.; Zhao, N.; Wang, S. Simultaneous adsorption of methyl orange and methylene blue from aqueous solution using amino functionalized Zr-based MOFs. *Microporous Mesoporous Mater.* **2019**, *282*, 179–187.

[27] Rathinam, K.; Singh, S. P.; Arnusch, C. J.; Kasher, R. An environmentally-friendly chitosan-lysozyme biocomposite for the effective removal of dyes and heavy metals from aqueous solutions. *Carbohydr. Polym.* **2018**, *199*, 506–515.

[28] Yu, Y.; Qiao, N.; Wang, D. J.; Zhu, Q. Z.; Fu, F.; Cao, R. Q.; Wang, R.; Liu, W.; Xu, B. Fluffy honeycomb-like activated carbon from popcorn with high surface area and well-developed porosity for ultra-high efficiency adsorption of organic dyes. *Bioresour. Technol.* **2019**, *285*, 121340.

[29] Islam, M. T.; Saenz-Arana, R.; Hernandez, C.; Guinto, T.; Ahsan, M. A.; Bragg, D. T.; Wang, H. Y.; Alvarado-Tenorio, B.; Noveron, J. C. Conversion of waste tire rubber into a high-capacity adsorbent for the removal of methylene blue, methyl orange, and tetracycline from water. *J. Environ. Chem. Eng.* **2018**, *6*, 3070–3082.

[30] Ji, W. J.; Hao, R. Q.; Pei, W. W.; Feng, L.; Zhai, Q. G. Design of two isoreticular Cd-biphenyltetracarboxylate frameworks for dye adsorption, separation and photocatalytic degradation. *Dalton Trans.* **2018**, *47*, 700–707.

[31] Embaby, M. S.; Elwany, S. D.; Setyaningsih, W.; Saber, M. R. The adsorptive properties of UiO-66 towards organic dyes: A record adsorption capacity for the anionic dye alizarin red S. *Chin. J. Chem. Eng.* **2018**, *26*, 731–739.

[32] Bahrudin, N. N.; Nawi, M. A.; Jawad, A. H.; Sabar, S. Adsorption characteristics and mechanistic study of immobilized chitosan-montmorillonite composite for methyl orange removal. *J. Polym. Environ.* **2020**, *28*, 1901–1913.

[33] Jiang, Y. Z.; Liu, B. C.; Xu, J. K.; Pan, K. L.; Hou, H. J.; Hu, J. P.; Yang, J. K. Cross-linked chitosan/β-cyclodextrin composite for selective removal of methyl orange: Adsorption performance and mechanism. *Carbohydr. Polym.* **2018**, *182*, 106–114.

[34] Vellingiri, K.; Szulejko, J. E.; Kumar, P.; Kwon, E. E.; Kim, K. H.; Deep, A.; Boukhvalov, D. W.; Brown, R. J. C. Metal organic frameworks as sorption media for volatile and semi-volatile organic compounds at ambient conditions. *Sci. Rep.* **2016**, *6*, 27813.

[35] Fan, S. J.; Guo, H.; Wang, Y. M.; Liu, J. H. Selective adsorption of the cationic dye rhodamine-6G from aqueous solution by phosphotungstic acid@MOF-199 composites. *J. Indian Chem. Soc.* **2022**, *99*, 100579.

[36] Mahmoodi, N. M.; Abdi, J. Nanoporous metal-organic framework (MOF-199): Synthesis, characterization and photocatalytic degradation of basic blue 41. *Microchem. J.* **2019**, *144*, 436–442.

[37] Wang, C. P.; Yin, H.; Tian, P. J.; Sun, X. J.; Pan, X. Y.; Chen, K. F.;

Chen, W. J.; Wu, Q. H.; Luo, S. Y. Remarkable adsorption performance of MOF-199 derived porous carbons for benzene vapor. *Environ. Res.* **2020**, *184*, 109323.

[38] Ma, Q.; Zhang, Q. Q.; Maimaiti, T.; Lan, S. K.; Liu, X. W.; Wang, Y. Q.; Li, Q.; Luo, H. Z.; Yu, B. W.; Yang, S. T. Carbonization reduces the toxicity of metal-organic framework MOF-199 to white-rot fungus *Phanerochaete chrysosporium*. *J. Environ. Chem. Eng.* **2021**, *9*, 106705.

[39] Fleming, I.; Williams, D. H. *Spectroscopic Methods in Organic Chemistry*; McGraw-Hill: London, 1966.

[40] Du, L.; Yang, J. Y.; Xu, X. R. Highly enhanced adsorption of dimethyl disulfide from model oil on MOF-199/attapulgite composites. *Ind. Eng. Chem. Res* **2019**, *58*, 2009–2016.

[41] Cyril, N.; George, J. B.; Joseph, L.; Sylas, V. P. Catalytic degradation of methyl orange and selective sensing of mercury ion in aqueous solutions using green synthesized silver nanoparticles from the seeds of *Derris trifoliata*. *J. Clust. Sci.* **2019**, *30*, 459–468.

[42] Kalyani, D. C.; Telke, A. A.; Govindwar, S. P.; Jadhav, J. P. Biodegradation and detoxification of reactive textile dye by isolated *Pseudomonas* sp. *SUK1*. *Water Environ. Res.* **2009**, *81*, 298–307.

[43] Ayed, L.; Khelifi, E.; Jannet, H. B.; Miladi, H.; Cheref, A.; Achour, S.; Bakhrouf, A. Response surface methodology for decolorization of azo dye methyl orange by bacterial consortium: Produced enzymes and metabolites characterization. *Chem. Eng. J.* **2010**, *165*, 200–208.

[44] Sun, Y. Y.; Yue, Q. Y.; Gao, B. Y.; Li, Q.; Huang, L. H.; Yao, F. J.; Xu, X. Preparation of activated carbon derived from cotton linter fibers by fused NaOH activation and its application for oxytetracycline (OTC) adsorption. *J. Colloid Interface Sci.* **2012**, *368*, 521–527.

[45] Newcombe, G.; Drikas, M. Adsorption of NOM onto activated carbon: Electrostatic and non-electrostatic effects. *Carbon* **1997**, *35*, 1239–1250.

[46] Chowdhury, Z. Z.; Zain, S. M.; Khan, R. A.; Islam, M. S. Preparation and characterizations of activated carbon from kenaf fiber for equilibrium adsorption studies of copper from wastewater. *Korean J. Chem. Eng.* **2012**, *29*, 1187–1195.

[47] Dirksen, A.; Zuidema, E.; Williams, R. M.; De Cola, L.; Kauffmann, C.; Vögtle, F.; Roque, A.; Pina, F. Photoactivity and pH sensitivity of methyl orange functionalized poly(propyleneamine) dendrimers. *Macromolecules* **2002**, *35*, 2743–2747.

[48] Song, X. L.; Liu, H. Y.; Cheng, L.; Qu, Y. X. Surface modification of coconut-based activated carbon by liquid-phase oxidation and its effects on lead ion adsorption. *Desalination* **2010**, *255*, 78–83.

[49] Moreno-Castilla, C.; Bautista-Toledo, I.; Ferro-Garcıa, M. A.; Rivera-Utrilla, J. Influence of support surface properties on activity of bacteria immobilised on activated carbons for water denitrification. *Carbon* **2003**, *41*, 1743–1749.

[50] Lagergren, S. Zur theorie der sogenannten adsorption geloster stoffe. *K. Sven. Vetenskapsakad. Handl.* **1898**, *24*, 1–39.

[51] Ho, Y. S.; McKay, G. Pseudo-second order model for sorption processes. *Process Biochem.* **1999**, *34*, 451–465.

[52] Simonin, J. P. On the comparison of pseudo-first order and pseudo-second order rate laws in the modeling of adsorption kinetics. *Chem. Eng. J.* **2016**, *300*, 254–263.